Preface

This book is based on my experience with the control systems of antennas and radiotelescopes. Overwhelmingly, it is based on experience with the NASA Deep Space Network (DSN) antennas. It includes modeling the antennas, developing control algorithms, field testing, system identification, performance evaluation, and troubleshooting. My previous book[1] emphasized the theoretical aspects of antenna control engineering, while this one describes the application part of the antenna control engineering.

Recently, the increased requirements for antenna/telescope pointing accuracy have been imposed. In the case of DSN antennas, it was the shift from the S-band (4 GHz) and X-band (8 GHz) communication to Ka band (32 GHz). On the other hand, the Large Millimeter Telescope will operate up to 200 GHz, which requires extremely accurate pointing. These requirements bring new challenges to the antenna control engineers. Classical PI controllers cannot assure the required accuracy, while model-based controllers (LQG, and H_∞) increase the antenna accuracy by a factor of 10. These controllers are new for antenna/telescope engineering. This book describes their development and application.

The book is addressed primarily to the antenna, telescope, and radiotelescope engineers, engineers involved in motion control, as well as students and researches in motion control and mechatronics (antenna is a combination of mechanical, power, and electronics subsystems). The book consists of two parts: Modeling (Chapters 2–5) and Control (Chapters 6–13).

In the modeling part, Chapter 2 describes the development of the analytical model of an antenna, including its structure (finite-element model) and drives (motors, reducers, amplifiers). This modeling is useful in the design stage of an antenna. Chapter 3 describes the determination of the antenna model using field tests and the system identification approach. These models are quite accurate, and are used in the development of the model-based controllers. Because the order of models (analytical as well as from the identification) is often too high for the analysis and

---

[1] Gawronski W. (2004). *Advanced Structural Dynamics, and Active Control of Structures.* Springer, New York.

for controller implementation, it is reduced to a reasonable size while preserving the critical properties of the full model. Chapter 4 briefly describes the reduction techniques as applied to antennas and telescopes. Finally, the wind disturbance models are developed in Chapter 5. Wind is the major disturbance source for antennas and telescopes. The steady (or static) wind model is presented, based on wind tunnel data and confirmed by the field data. Also, three wind gusts models are presented.

The control part presents the performance criteria and shows how to transform the antenna model to be the most suitable for controller tuning. In Chapter 7, the book presents the development, properties, and limitations of the PI controller. It shows the impact of the proportional and the integral gains on the antenna closed-loop performance. It also analyzes the limits of the PI controller performance. Chapter 8 describes the tuning process of the LQG controller. It analyzes the performance of the LQG controller, including its limits. It presents the graphical user interface (GUI) that allows us to tune the antenna LQG controller without analysis, but by playing with the GUI sliders and buttons ("LQG for dummies"). It is shown in this chapter that the performance of the LQG controller depends on its location: either at the position loop or at the velocity loop, or at both. It shows also that in the case of the 34-m DSN antennas the servo error with LQG controller decreased by a factor of 6.5 when compared to the PI controller. In Chapter 9, H_∞ controller tuning is presented: gain determination, closed-loop equations, limits of performance. In the following chapter, the non-linear control issues are addressed. The velocity and acceleration limits often interfere with antenna dynamics. Two solutions are proposed: a command preprocessor, and the anti-windup technique. Friction is the source of a deteriorated pointing. Dither can be a solution, as presented in this book. Finally, gearbox backlash is described and the counter-torque solution to minimize it is presented.

A typical antenna control system consists of two loops: velocity and position loops. A single-loop solution is studied in Chapter 11. The antenna control system uses the encoder measurements to estimate RF beam position, but it is only a rough estimate. The encoder measures the antenna angular position at its location, which is different from the RF beam location; thus, antenna structural compliance is the source of the error. Chapter 12 describes two techniques to control the RF beam position: monopulse and conscan. Finally, in Chapter 13 we describe an open-loop RF beam control: the look-up table that corrects for the uneven azimuth track that impacts the RF beam position.

Analysis is a skill. However, even complex theories and the supporting analysis are, in a sense, simple because they assume certain properties that simplify the analysis, or to make it possible. Still, although the theoretical path delivers an answer, engineers have to ask if the answer is applicable to the real environment.

Engineering is an art. Some aspects of engineering can be described rigorously by theoretical analysis, but not all. There are cases where engineering reality does not satisfy analytical assumptions. Hence, engineering solutions are often ad hoc solutions. This engineering dilemma is summarized by Scholnik: "Who cares how it works, just as long as it gives the right answer."

The art of engineering often includes features that theoretically cannot work. For example:

- LQG controllers cannot be applied to antennas, because the antenna model have poles at zero (rigid-body mode). But the LQG controllers do control the antennas.
- The noise in the tuning of the LQG controller should be the Gaussian noise, which is not the case of antennas or telescopes.
- Rigidly applied model reduction algorithms do not produce the best reduced model (best in terms of the antenna performance).
- Every LQG controller is an optimal controller, but not every one is acceptable.
- In the H_∞ controller tuning the plant uncertainity should be either additive or multiplicative. The antenna uncertainity, which depends on its elevation position, is neither additive nor multiplicative.

Despite these difficulties, engineers succeed in developing acceptable control systems, including antennas and telescopes.

Readers who would like to contact me with comments and questions are invited to do so. My e-mail address is wodek.k.gawronski@jpl.nasa.gov or w.gawronski@sbcglobal.net.

W. Gawronski
Pasedena, California

Acknowledgements

Part of the work described in this book was carried out at the Jet Propulsion Laboratory, California Institute of Technology, under contract with the National Aeronautics and Space Administration. I thank Alaudin Bhanji, Mark Gatti, Pete Hames, Wendy Hodgin, Andre Jongeling, Scott Morgan, Jean Patterson, Daniel Rascoe, Christopher Yung, and Susan Zia, the managers at the Communications Ground Systems Section, Jet Propulsion Laboratory, for their support of the Deep Space Network antenna study.

I would like to acknowledge the contributions of my colleagues who have had an influence on this work:

- from the Jet Propulsion Laboratory: Harlow Ahlstrom, Mimi Aung, Farrokh Baher, Abner Bernardo, John Cucchissi, Jeffery Mellstrom, Martha Strain;
- from the NASA Goldstone Deep Space Communication Complex (California): Michael Winders and Jeffrey Frazier;
- from the NASA Madrid Deep Space Communication Complex (Spain): Angel Martin, David Munoz Mochon, and Pablo Perez-Zapardiel;
- from the NASA Canberra Deep Space Communication Complex (Australia): Paul Richter and John Howell;
- visiting students: Jason Brand, Emily Craparo, Brandon Kuczenski, and Erin Maneri whose work is also included in this book.

I also acknowledge the help of Kamal Souccar in the study of the Large Millimeter Telescope; Bogusz Bienkiewicz of Colorado State University in the wind disturbance study; and Toomas Erm of the European Southern Observatory, Munich, Germany, for many interesting discussions on control systems of antennas and telescopes.

Chapter 2
Analytical Models

This chapter presents the development of the analytical model of the antenna velocity loop. The analytical model includes the antenna structure, its drives, and the velocity loop itself. First, a rigid antenna model is discussed. Next, the modal model of a flexible antenna structure is analyzed based on the finite-element data. The modal model is transferred into the state-space model, in both continuous- and discrete-time. Next, the drive model is derived, and combined into the velocity loop model. Finally, the impact of the drive parameters (gearbox stiffness and motor inertia) on the velocity loop properties is analyzed. It is worth to remind that the analytical model is mainly used in the design stage of the antenna. Due to limited accuracy of the analytical modeling, these models cannot be used in implementation, such as the model-based controllers.

2.1 Rigid Antenna Model

In this section the velocity loop of a rigid-body antenna is analyzed. Such models represents an antenna without flexible deformations in the disturbance frequency band, and are well beyond antenna bandwidth. This is a model of an idealized antenna, with rigid gearboxes and a rigid structure. It might be applicable to small antennas, but in our case it serves as a tool for explaining and deriving basic velocity loop properties in a closed form (while for larger, flexible antennas the analysis is based on Matlab and Simulink simulations). This simple analysis is extended later to illustrate properties of a flexible antenna control system, and for the better insight into more complicated models and their properties.

A rigid antenna in the open loop configuration has torque input and velocity output. The relationship between the torque τ and angular velocity ω follows from the Newton inertia law

$$J\dot{\omega} = \tau \tag{2.1}$$

where J is the antenna inertia. The Laplace transform of the above equation is $Js\omega(s) = \tau(s)$; hence, the antenna transfer function is represented as an integrator

W. Gawronski, *Modeling and Control of Antennas and Telescopes*,
DOI: 10.1007/978-0-387-78793-0_2, © Springer Science+Business Media, LLC 2008

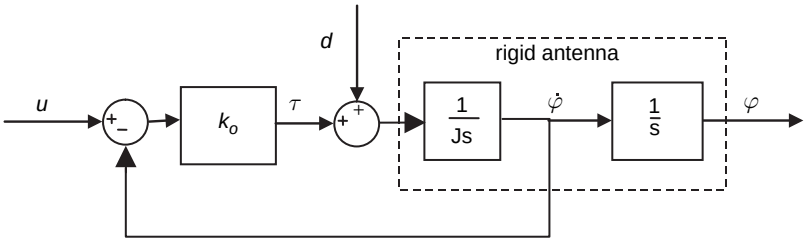

Fig. 2.1 Velocity loop model of a rigid antenna

$$G(s) = \frac{\omega(s)}{\tau(s)} = \frac{1}{Js} \tag{2.2}$$

The velocity loop model of a rigid antenna with a proportional controller is shown in Fig. 2.1. The transfer function of the closed velocity loop system, from the velocity command u to the antenna velocity $\dot{\varphi}$, is as follows:

$$G_{rl}(s) = \frac{\dot{\varphi}(s)}{u(s)} = \frac{k_o G(s)}{1 + k_o G(s)} = \frac{1}{1 + Ts} \tag{2.3}$$

where $T = J/k_o$. The bandwidth of the velocity loop system is equal to $B = 1/T = k_o/J$ rad/s. The gain, k_o, is tuned to obtain the required bandwidth of the system. For example, if the required bandwidth is $B = 20$ rad/s, and the inertia is $J = 1$ Nms^2/rad, then $k_o = 20$ Nms.

2.2 Structural Model

The structural model is typically derived from the finite-element model. It is not the finite-element model per se, but its by-product, the modal model. Note that the modal model includes the rigid-body mode (antenna-free rotation). For the controller tuning purposes the modal model is represented in state-space form, which it is finally given in the discrete-time representation.

2.2.1 Finite-Element Model

The analytical model of an antenna is obtained from its finite-element model. The finite element model of a 34-m antenna is shown in Fig. 2.2. It consists of hundreds of nodes and elements, and thousands of degrees of freedom. The model is characterized by the mass, stiffness, and damping matrices, and by the sensors and actuator locations.

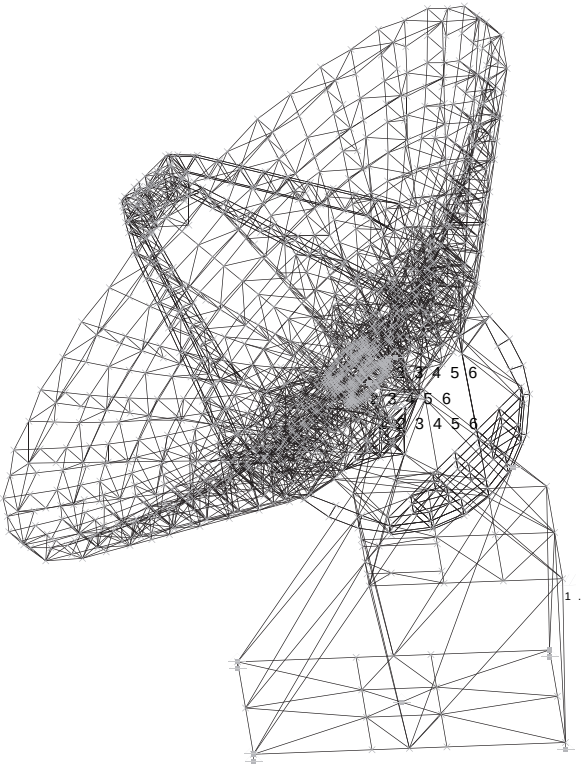

Fig. 2.2 The finite-element model of the 34-m antenna

Let N be a number of degrees of freedom of the finite-element model, with antenna displacement and velocity at the encoder location as the output and force at the motor pinion attachment as the input. Antenna structure is represented by the following second-order matrix differential equation:

$$\begin{aligned} M\ddot{q} + D\dot{q} + Kq &= B_o u, \\ y &= C_{oq} q + C_{ov} \dot{q}. \end{aligned} \tag{2.4}$$

In this equation q is the $N \times 1$ nodal displacement vector; $\dot{q}$ is the $N \times 1$ nodal velocity vector; $\ddot{q}$ is the $N \times 1$ nodal acceleration vector; u is the input; y is the output; M is the mass matrix, $N \times N$; D is the damping matrix, $N \times N$; and K is the stiffness matrix, $N \times N$. The input matrix B_o is $N \times 1$, the output displacement matrix C_{oq} is $1 \times N$, and the output velocity matrix C_{ov} is $1 \times N$. The mass matrix is positive definite (all its eigenvalues are positive), and the

stiffness and damping matrices are positive semi-definite (all their eigenvalues are non-negative).

2.2.2 Modal Model

Modal models of antennas are expressed in modal coordinates. Because these coordinates are independent, they simplify the analysis. The modal model is obtained by transforming equation (2.4) using a modal matrix; see [2].

Consider free vibrations of an antenna structure without damping, and without external excitation, that is, $u = 0$ and $D = 0$. The equation of motion (2.4) in this case turns into the following equation:

$$M\ddot{q} + Kq = 0. \tag{2.5}$$

The solution of the above is $q = \phi e^{j\omega t}$; hence, the second derivative of the solution is $\ddot{q} = -\omega^2 \phi e^{j\omega t}$. Introducing q and $\ddot{q}$ into (2.5) gives

$$(K - \omega^2 M)\phi e^{j\omega t} = 0. \tag{2.6}$$

This set of homogeneous equations has a nontrivial solution if the determinant of $K - \omega^2 M$ is zero, that is,

$$\det(K - \omega^2 M) = 0. \tag{2.7}$$

The above determinant equation is satisfied for a set of n values of frequency ω. These frequencies are denoted $\omega_1, \omega_2, ..., \omega_n$, and their number n does not exceed the number of degrees of freedom, i.e., $n \leqslant N$. The frequency ω_i is called the ith natural frequency.

Substituting ω_i into (2.6) yields the corresponding set of vectors $\{\phi_1, \phi_2, ..., \phi_n\}$ that satisfy this equation. The ith vector ϕ_i corresponding to the ith natural frequency is called the ith mode shape. The natural modes are not unique, since they can be arbitrarily scaled. Indeed, if ϕ_i satisfies (2.6), so does $\alpha\phi_i$, where α is an arbitrary scalar.

For a notational convenience define the matrix of natural frequencies

$$\Omega = \begin{bmatrix} \omega_1 & 0 & \cdots & 0 \\ 0 & \omega_2 & \cdots & 0 \\ \cdots & \cdots & \cdots & \cdots \\ 0 & 0 & \cdots & \omega_n \end{bmatrix} \tag{2.8}$$

and the matrix of mode shapes, or modal matrix Φ, of dimensions $N \times n$, which consists of n natural modes of a structure

$$\Phi = \left[\begin{array}{cccc} \phi_1 & \phi_2 & \ldots & \phi_n \end{array} \right] = \left[\begin{array}{cccc} \phi_{11} & \phi_{21} & \cdots & \phi_{n1} \\ \phi_{12} & \phi_{22} & \cdots & \phi_{n2} \\ \cdots & \cdots & \cdots & \cdots \\ \phi_{1k} & \phi_{2k} & \cdots & \phi_{nk} \\ \cdots & \cdots & \cdots & \cdots \\ \phi_{1n_d} & \phi_{2n_d} & \cdots & \phi_{nn_d} \end{array} \right], \tag{2.9}$$

where ϕ_{ij} is the jth displacement of the ith mode, that is,

$$\phi_i = \left\{ \begin{array}{c} \phi_{i1} \\ \phi_{i2} \\ \vdots \\ \phi_{in} \end{array} \right\}. \tag{2.10}$$

The modal matrix Φ has an interesting property: it diagonalizes mass and stiffness matrices M and K,

$$M_m = \Phi^T M \Phi, \qquad K_m = \Phi^T K \Phi. \tag{2.11}$$

The obtained diagonal matrices are called modal mass matrix (M_m) and modal stiffness matrix (K_m), respectively. The same transformation, applied to the damping matrix

$$D_m = \Phi^T D \Phi, \tag{2.12}$$

gives the modal damping matrix D_m, which is a diagonal if it is, for example, proportional to the stiffness matrix.

In order to obtain the modal model a new variable, q_m, is introduced. It is called modal displacement, and satisfies the following equation:

$$q = \Phi q_m. \tag{2.13}$$

Equation (2.13) is introduced to (2.4), and the latter additionally left-multiplied by Φ^T, obtaining

$$\begin{aligned} &M_m \ddot{q}_m + D_m \dot{q}_m + K_m q_m = \Phi^T B_o u, \\ &y = C_{oq} \Phi q_m + C_{ov} \Phi \dot{q}_m. \end{aligned}$$

using (2.11), and (2.12) notations. Next, the left multiplication of the latter equation by M_m^{-1}, which gives

$$\begin{aligned} &\ddot{q}_m + 2\mathrm{Z}\Omega\dot{q}_m + \Omega^2 q_m = B_m u, \\ &y = C_{mq} q_m + C_{mv}\dot{q}_m. \end{aligned} \tag{2.14}$$

In (2.14) Ω is a diagonal matrix of natural frequencies, defined before, and Z is the modal damping matrix. It is a diagonal matrix of modal damping,

$$\mathrm{Z} = \begin{bmatrix} \zeta_1 & 0 & \cdots & 0 \\ 0 & \zeta_2 & \cdots & 0 \\ \cdots & \cdots & \cdots & \cdots \\ 0 & 0 & \cdots & \zeta_n \end{bmatrix}. \tag{2.15}$$

where ζ_i is the damping of the ith mode. This matrix is obtained using the following relationship $M_m^{-1} D_m = 2\mathrm{Z}\Omega$, thus,

$$\mathrm{Z} = 0.5 M_m^{-1} D_m \Omega^{-1} = 0.5 M_m^{-\frac{1}{2}} K_m^{-\frac{1}{2}} D_m. \tag{2.16}$$

The modal input matrix B_m in (2.14) is as follows

$$B_m = M_m^{-1} \Phi^T B_o. \tag{2.17}$$

Finally, in (2.14) the following notations is used for the modal displacement and velocity matrices:

$$C_{mq} = C_{oq}\Phi, \tag{2.18}$$

$$C_{mv} = C_{ov}\Phi. \tag{2.19}$$

Note that (2.14) (a modal representation of a structure) is a set of uncoupled equations. Indeed, due to the diagonality of Ω and Z, this set of equations can be written, equivalently, as

$$\begin{aligned} &\ddot{q}_{mi} + 2\zeta_i \omega_i \dot{q}_{mi} + \omega_i^2 q_{mi} = b_{mi} u \\ &y_i = c_{mqi} q_{mi} + c_{mvi}\dot{q}_{mi}, \qquad i = 1, \ldots, n, \\ &y = \sum_{i=1}^{n} y_i, \end{aligned} \tag{2.20}$$

where b_{mi} is the ith row of B_m and c_{mqi}, c_{mvi} are the ith columns of C_{mq} and C_{mv}, respectively. In the above equations y_i is the system output due to the ith mode dynamics. Note that the structural response y is a sum of modal responses y_i, which is a key property used to derive structural properties in modal coordinates.

Theoretically the determination of the input and output matrices as in (2.17), (2.18), and (2.19) requires large matrix Φ (of size: number of degrees of freedom

by number of modes). In fact, one needs only one row of it for each input/output matrix. Indeed, the input matrix B_o is all zero, except the location of the actuator (pinion) to the structure. The same, the output matrix C_{mq} is all zero, except the location of the sensor (encoder) to the structure. Let the location of the sensor is at the kth degree of freedom of the finite-element model. The modal matrix is as in (2.9). Because C_{mq} is all zero but the kth entry, therefore

$$C_{mq} = C_{oq}\Phi = \begin{bmatrix} 0\ 0\ \ldots\ 1\ \ldots\ 0 \end{bmatrix} \begin{bmatrix} \phi_{11} & \phi_{21} & \ldots & \phi_{n1} \\ \phi_{12} & \phi_{22} & \ldots & \phi_{n2} \\ \ldots & \ldots & \ldots & \ldots \\ \phi_{1k} & \phi_{2k} & \ldots & \phi_{nk} \\ \ldots & \ldots & \ldots & \ldots \\ \phi_{1n_d} & \phi_{2n_d} & \ldots & \phi_{nn_d} \end{bmatrix} = \begin{bmatrix} \phi_{1k}\ \phi_{2k}\ \ldots\ \phi_{nk} \end{bmatrix} \tag{2.21}$$

that is, C_{mq} consists of modal displacement at the encoder location. Similarly, if the actuator (pinion) is located at the kth degree of freedom, the corresponding input matrix is

$$B_{mq} = \begin{bmatrix} \phi_{1k}/m_{m1} \\ \phi_{2k}/m_{m2} \\ \cdots \\ \phi_{nk}/m_{mn} \end{bmatrix} \tag{2.22}$$

where m_{mi} is the ith modal mass. Thus, B_{mq} consists of modal displacement at the actuator (pinion) location scaled by the modal masses.

In summary, from comparatively few parameters of the finite-element model, such as natural frequencies, modal masses, modal damping, and modal displacements at the actuator and sensor locations one creates the antenna structural model in equation (2.14). Note that this structural dynamics model of an antenna is much simpler than its static finite-element model.

As an example, determine the first four natural modes and frequencies of the antenna presented in Fig. 2.2. The modes are shown in Fig. 2.3. For the first mode the natural frequency is $\omega_1 = 13.2$rad/s (2.10 Hz), for the second mode the natural frequency is $\omega_2 = 18.1$ rad/s (2.88 Hz), for the third mode the natural frequency is $\omega_3 = 18.8$ rad/s (2.99 Hz), and for the fourth mode the natural frequency is $\omega_4 = 24.3$ rad/s (3.87 Hz).

2.2.3 State-Space Model

State-space representation is the standard representation of the control system models. Thus, the antenna structure needs to be represented in this form, to allow the use of control system software such as Matlab or Simulink. The modal state-space

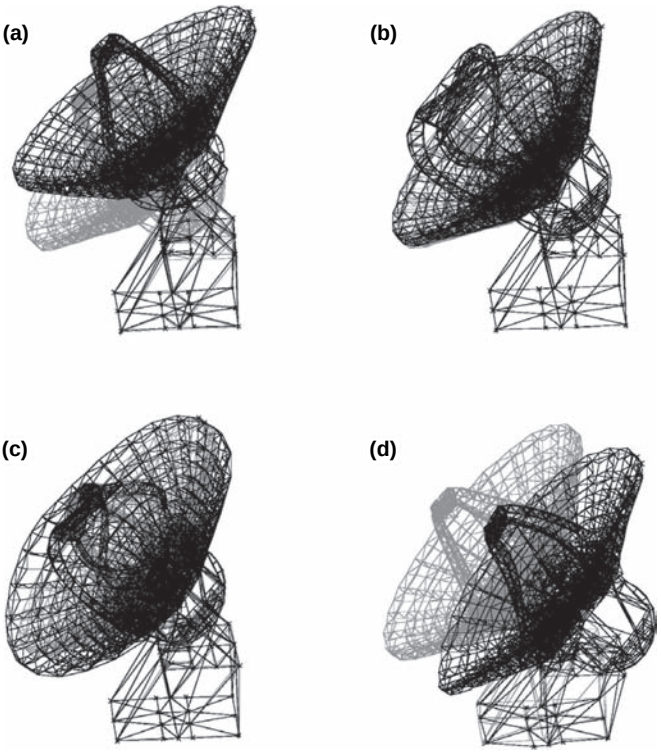

Fig. 2.3 Antenna modes: (**a**) First mode (of natural frequency 2.10 Hz); (**b**) second mode (of natural frequency 2.87 Hz); (**c**) third mode (of natural frequency 2.99 Hz); and (**d**) fourth mode (of natural frequency 3.87 Hz). For each mode the nodal displacements are sinusoidal, have the same frequency, and the displacements are shown at their extreme values. Gray color denotes undeformed state

representation of the antenna structure is a triple (A_m, B_m, C_m) characterized by the block-diagonal state matrix, A_m; see [2]

$$A_m = \mathrm{diag}(A_{mi}) = \left[\begin{array}{cc:cc:ccc:cc} \times & \times & 0 & 0 & \cdots & \cdots & 0 & 0 \\ \times & \times & 0 & 0 & \cdots & \cdots & 0 & 0 \\ \hdashline 0 & 0 & \times & \times & \cdots & \cdots & 0 & 0 \\ 0 & 0 & \times & \times & \cdots & \cdots & 0 & 0 \\ \hdashline \cdots & \cdots & \cdots & \cdots & \cdots & \cdots & \cdots & \cdots \\ \cdots & \cdots & \cdots & \cdots & \cdots & \cdots & \cdots & \cdots \\ \hdashline 0 & 0 & 0 & 0 & \cdots & \cdots & \times & \times \\ 0 & 0 & 0 & 0 & \cdots & \cdots & \times & \times \end{array}\right], \quad i = 1, 2, \ldots, n, \tag{2.23}$$

where A_{mi} are 2×2 blocks (their nonzero elements are marked with $\times$), and the modal input and output matrices are divided, correspondingly,

$$B_m = \begin{bmatrix} B_{m1} \\ B_{m2} \\ \vdots \\ B_{mn} \end{bmatrix}, \qquad C_m = \begin{bmatrix} C_{m1} \; C_{m2} \cdots \; C_{mn} \end{bmatrix}, \tag{2.24}$$

The blocks A_{mi}, B_{mi}, and C_{mi} are as follows:

$$A_{mi} = \begin{bmatrix} 0 & \omega_i \\ -\omega_i & -2\zeta_i\omega_i \end{bmatrix}, \qquad B_{mi} = \begin{bmatrix} 0 \\ b_{mi} \end{bmatrix}, \qquad C_{mi} = \begin{bmatrix} \frac{c_{mqi}}{\omega_i} & c_{mvi} \end{bmatrix}; \tag{2.25}$$

The state x of the modal representation consists of n independent components, x_i, that represent a state of each mode

$$x = \begin{Bmatrix} x_1 \\ x_2 \\ \vdots \\ x_n \end{Bmatrix}, \tag{2.26}$$

The ith state component is as follows:

$$x_i = \begin{Bmatrix} \omega_i q_{mi} \\ \dot{q}_{mi} \end{Bmatrix}, \tag{2.27}$$

The ith component, or mode, has the state-space representation (A_{mi}, B_{mi}, C_{mi}) independently obtained from the state equations

$$\begin{aligned} \dot{x}_i &= A_{mi}x_i + B_{mi}u, \\ y_i &= C_{mi}x_i, \\ y &= \sum_{i=1}^{n} y_i. \end{aligned} \tag{2.28}$$

This decomposition is justified by the block-diagonal form of the matrix A_m,

The poles of a structure are the zeros of the characteristic equations . The equation $s^2 + 2\zeta_i\omega_i s + \omega_i^2 = 0$ is the characteristic equation of the ith mode. For small damping the poles are complex conjugate, and in the following form:

$$s_{1,2} = -\zeta_i\omega_i \pm j\omega_i\sqrt{1-\zeta_i^2}. \tag{2.29}$$

The plot of the poles is shown in Fig. 2.4, which shows how the location of a pole relates to the natural frequency and modal damping.

2.2.4 Models with Rigid Body Modes

Antenna structure is unrestrained—it can free rotate with respect to azimuth and elevation axes. Modal analysis for such structures shows that they have zero natural frequency, and that the corresponding natural mode shows structural displacements

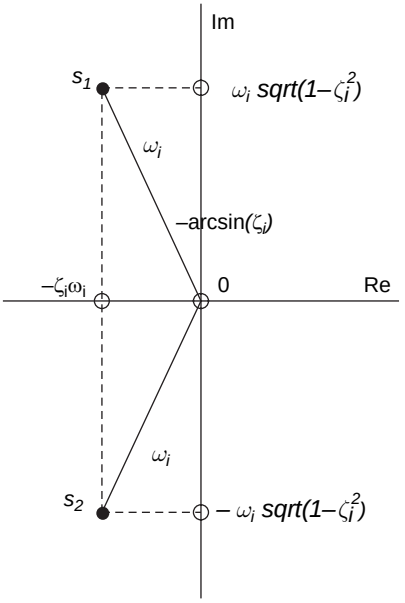

Fig. 2.4 Pole location of the *i*th mode of a lightly damped structure: It is a complex pair with the real part proportional to the *i*th modal damping; the imaginary part approximately equal to the *i*th natural frequency; and the radius is the exact natural frequency

but no flexible deformations. A mode without flexible deformations is called a rigid-body mode. Corresponding zero frequency implies that the zero frequency harmonic excitation (which is a constant force or torque) causes rigid-body movement of the structure. Structural analysts sometimes ignore this mode, as there is no deformation involved. However, it is of crucial importance for a control engineer, because this mode is the one that allows a controller to move a structure and track a command.

The rigid-body modes are obtained by solving the same eigenvalue problem as presented for the standard models. Because the natural frequency is zero, the modal equation becomes $\det(K) = 0$, that is, the stiffness matrix becomes singular. The corresponding rigid-body mode ϕ_{rb} is the one that satisfies the equation

$$K\phi_{rb} = 0. \tag{2.30}$$

The modal equations for the rigid-body modes follow from (2.20) by assuming $\omega_i = 0$, that is,

$$\begin{aligned} \ddot{q}_{mi} &= b_{mi}u, \\ y_i &= c_{mqi}q_{mi} + c_{mvi}\dot{q}_{mi}, \\ y &= \sum_{i=1}^{n} y_i. \end{aligned} \tag{2.31}$$

The state-space modal model for a rigid-body mode is as follows,

$$A_{mi} = \begin{bmatrix} 0 & 1 \\ 0 & 0 \end{bmatrix}, \qquad B_{mi} = \begin{bmatrix} 0 \\ b_{mi} \end{bmatrix}, \qquad C_{mi} = \begin{bmatrix} c_{mqi} & c_{mvi} \end{bmatrix}, \tag{2.32}$$

For the experienced engineer the rigid-body frequency and mode are not difficult to determine: rigid-body frequency is always zero, and rigid-body mode can be predicted as a structural movement without deformation. The importance of distinguishing it from "regular" modes is the fact that they make a system unstable, and thus a system that requires special attention.

The Deep Space Network antenna has two rigid-body modes: rigid-body rotation with respect to the azimuth (vertical) axis, and rigid-body rotation with respect to the elevation (horizontal) axis. Figure 2.5 shows the azimuth rigid-body mode. Figure 2.5(a) presents the initial position from the top view; Fig. 2.5(b) presents the modal displacement (rigid-body rotation with respect to the azimuth axis) from the top view,

2.2.5 Discrete-Time Model

For the antenna performance simulations and for the controller tuning purposes the discrete-time models are required. The discrete time model is obtained from a continuous-time state-space representation (A,B,C). Because the discrete-time sequences of this model are sampled continuous-time signals, that is,

$$x_k = x(k\Delta t), \qquad u_k = u(k\Delta t), \text{ and } y_k = y(k\Delta t), \tag{2.33}$$

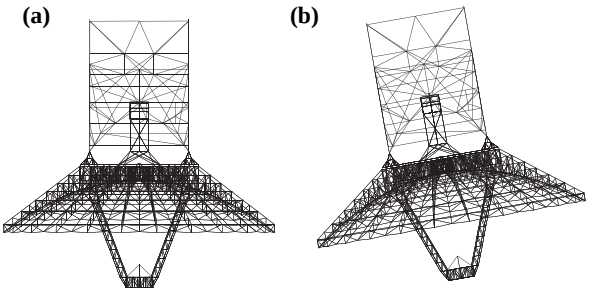

Fig. 2.5 Antenna in neutral position (**a**), and the azimuth rigid-body mode (**b**), where no flexible deformations are observed

for $k = 1, 2, 3 \ldots$, thus the corresponding discrete-time representation for the sampling time Δt is (A_d, B_d, C_d, D_d), where

$$A_d = e^{A\Delta t}, \qquad B_d = \int_0^{\Delta t} e^{A\tau} B d\tau, \qquad C_d = C, \tag{2.34}$$

and the corresponding state-space equations are

$$\begin{aligned} x_{k+1} &= A_d x_k + B_d u_k, \\ y_k &= C x_k. \end{aligned} \tag{2.35}$$

The discretization can be carried out numerically using the *c2d* command of Matlab.

Next, the discrete-time models is presented in modal coordinates. Assume small damping and the sampling rate sufficiently fast, such that the Nyquist sampling theorem is satisfied (i.e., $\omega_i \Delta t \leqslant \pi$ for all i), see, for example, [1, p. 111], then the state matrix in modal coordinates A_{dm} is block-diagonal,

$$A_{dm} = \text{diag}(A_{dmi}), \qquad i = 1, \ldots, n. \tag{2.36}$$

The 2×2 blocks A_{dmi} are in the form (see [4]),

$$A_{dmi} = e^{-\zeta_i \omega_i \Delta t} \begin{bmatrix} \cos(\omega_i \Delta t) & -\sin(\omega_i \Delta t) \\ \sin(\omega_i \Delta t) & \cos(\omega_i \Delta t) \end{bmatrix}, \tag{2.37}$$

where ω_i and ζ_i are the ith natural frequency and the ith modal damping, respectively. The modal input matrix B_{dm} consists of 2×1 blocks B_{dmi},

$$B_{dm} = \begin{bmatrix} B_{dm1} \\ B_{dm2} \\ \vdots \\ B_{dmn} \end{bmatrix}, \tag{2.38}$$

where

$$B_{dmi} = S_i B_{mi}, \qquad S_i = \frac{1}{\omega_i} \begin{bmatrix} \sin(\omega_i \Delta t) & -1 + \cos(\omega_i \Delta t) \\ 1 - \cos(\omega_i \Delta t) & \sin(\omega_i \Delta t) \end{bmatrix}, \tag{2.39}$$

and B_{mi} is the continuous-time modal representation. The discrete-time modal matrix C_{dm} is the same as the continuous-time modal matrix C_m.

The poles of the matrix A_{dm} are composed of the poles of matrices A_{dmi}, $I = 1,\ldots, n$. For the ith mode the poles of A_{dmi} are

$$s_{1,2} = e^{-\zeta_i \omega_i \Delta t}(\cos(\omega_i \Delta t) \pm \sin(\omega_i \Delta t)). \tag{2.40}$$

The location of the poles is shown in Fig. 2.6, which is quite different from the continuous-time system, cf., Fig. 2.5. For a stable system they should be inside the unit circle.

The question arises how to choose the sampling time Δt. Note that from the Nyquist criterion the ith natural frequency is recovered if the sampling rate is at least twice the natural frequency in Hz ($f_i = \omega_i / 2\pi$), that is, if

$$\frac{1}{\Delta t} \geqslant 2 f_i$$

or, if

$$\omega_i \Delta t \leqslant \pi \qquad \text{or} \qquad \Delta t \leqslant \frac{\pi}{\omega_i}. \tag{2.41}$$

Considering all modes, the sampling time will be smaller than the smallest π / ω_i,

$$\Delta t \leqslant \frac{\pi}{\max\limits_i(\omega_i)}. \tag{2.42}$$

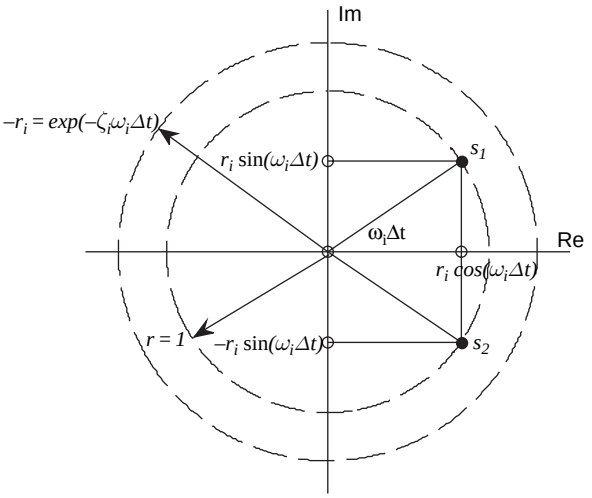

Fig. 2.6 Pole location of the ith mode of a lightly damped structure in discrete time: It is a complex pair with angle proportional to natural frequency and magnitude close to 1

2.3 Drive Model

The drive model consists of motor, reducer, amplifiers, and tachometers.

2.3.1 Motor Model

The motor model is shown in Fig. 2.7. The motor position (θ_m) is controlled by the armature voltage (v_a)

$$v_a = L_a \frac{di_o}{dt} + R_a i_o + k_b \omega_m \tag{2.43}$$

where R_a is motor resistance, L_a is motor inductance, and k_b is the armature constant. The motor torque (T_o) is proportional to the motor current (i_o)

$$T_o = k_m i_o \tag{2.44}$$

where k_m is the motor torque constant. The motor torque, T_o is in equilibrium with the remaining torque acting on the rotor; therefore,

$$T_o = J_m \ddot{\theta}_m + T \tag{2.45}$$

where T is the drive output torque, and J_m is a total inertia of the motor and the brake.

The above equations give the following (after Laplace transform, where s is the Laplace variable)

$$i_o = \frac{v_a - k_b \omega_m}{L_a s + R_a}$$

$$\omega_m = \frac{1}{J_m s}(T_o - T)$$

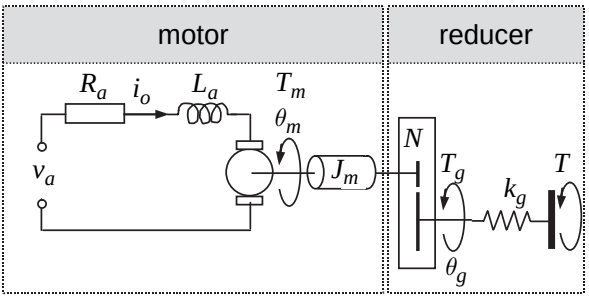

Fig. 2.7 Motor and reducer model

2.3.2 Reducer Model

The reducer model is shown in Fig. 2.7 as well. The torque T at the output of the gearbox can be expressed with the torsional deformation of the gearbox

$$T = k_g(\theta_g - \theta_p) \tag{2.46}$$

θ_p is the angle of rotation of the pinion, k_g is the stiffness of the reducer and drive shaft, N is the reducer gear ratio, θ_g is the angle of rotation of the reducer output shaft

$$\theta_g = \frac{\theta_m}{N} \tag{2.47}$$

2.3.3 Drive Model

Based on the above equations the drive model (e.g., Simulink) is created. Besides motor and reducer, amplifiers are added. A block-diagram of the drive is created; see Fig. 2.8. The parameters of this model are given in Table 2.1.

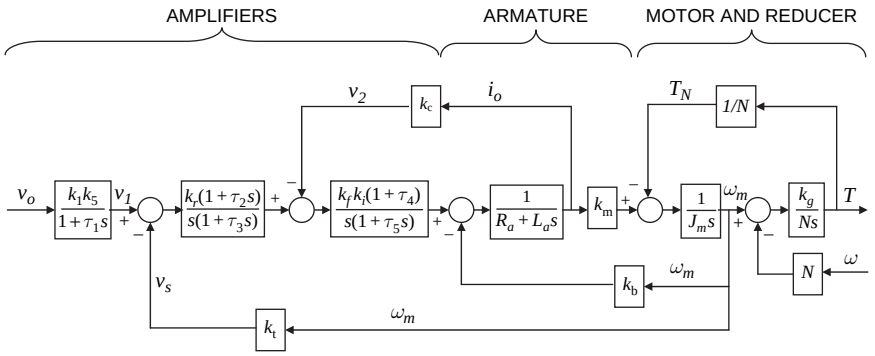

Fig. 2.8 Block diagram of the drive model

Table 2.1 Drive parameters

k_1 = 716.2	[V s/rad]	k_f = 54 [-]	[-]	τ_1 = 0.00637	[s]
k_m = 1.787	[Nm/A]	k_g = 1.7× 10^6	[Nm/rad]	τ_2 = 0.094	[s]
k_b = 1.79	[V s/rad]	J_m = 0.14	[Nm/s^2]	τ_3 = 0.002	[s]
k_s = 0.8	[-]	R_a = 0.456	[Ω]	τ_4 = 0.00484	[s]
k_t = 0.0384	[V s/rad]	L_a = 0.011	[H]	τ_5 = 0.0021	[s]
k_r = 80	[V/s/V]	N = 354	[-]	τ_6 = 0.7304	[s]
k_c = 0.1266	[V/A]				

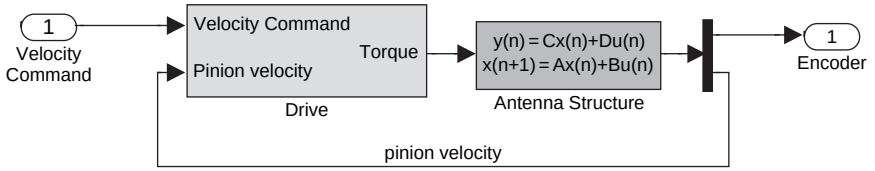

Fig. 2.9 Velocity loop model

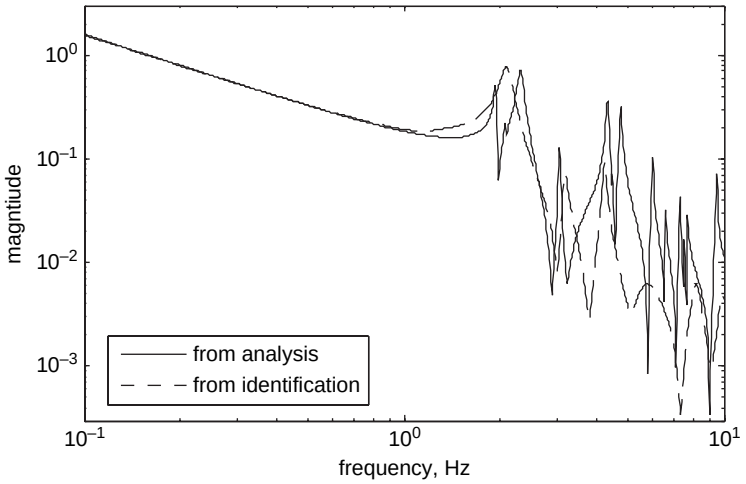

Fig. 2.10 The magnitude of the transfer function of the velocity loop model

2.4 Velocity Loop Model

The Simulink velocity loop model is a combination of the structural and drive models; see Fig. 2.9. The drive torque moves the antenna. The pinion velocity is fed back to the drive to calculate the reducer flexible deformation. The velocity command controls the antenna velocity, and the encoder measures its position.

The magnitude of the velocity loop transfer function is shown in Fig. 2.10, solid line.

2.5 Drive Parameter Study

In this section the effect of the drive inertia and stiffness on the antenna velocity loop properties is investigated. The inertia of the drive includes motor, brake, and gearbox, and the drive stiffness includes gearbox stiffness and shaft stiffness. Because the motor dominates the drive inertia, the motor inertia is investigated, and because gearbox stiffness dominates the drive stiffness, the drive stiffness is investigated.

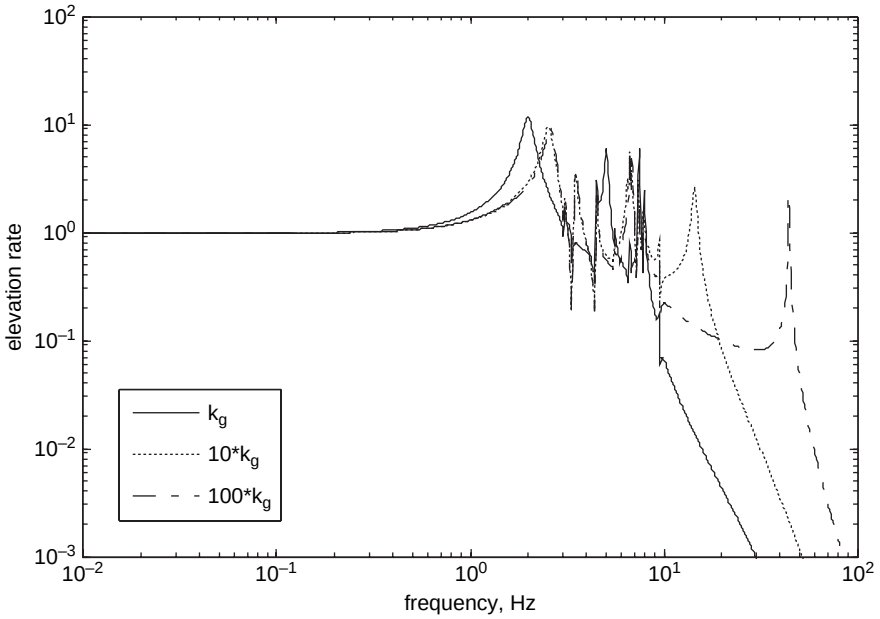

Fig. 2.11 The magnitudes of the transfer function of the velocity loop model for the nominal and increased gearbox stiffness

It is intuitively obvious that a rigid gearbox and a powerful but weightless motor are the best choice for the antenna drive (if they exist). So, what is the smallest allowable gearbox stiffness, or the largest allowable motor inertia? The 34-m antenna velocity loop bandwidth is simulated as a function of motor inertia, and as a function of the gearbox stiffness [3], using the model as in Fig. 2.8 and Fig. 2.9. The nominal motor inertia is 0.14 [Nms^2], and the nominal gearbox stiffness is 1.7×10^6 [N m/rad]; see Table 2.1. The transfer function, from the velocity command to the output velocity for the nominal values, is shown in Fig. 2.11, solid line.

2.5.1 Drive Stiffness Factor

The impact of the gearbox stiffness on the velocity loop properties is simulated, for the nominal gearbox stiffness and for increased stiffness by factors of 10 and 100, respectively. The corresponding transfer functions are shown in Fig. 2.11, dotted (for factor 10) and dot-dashed lines (for factor 100), respectively. One can see that the transfer function bandwidth changed when k_g incresed to $10k_g$. The resonant peak, related to the drive vibration mode shifted to higher frequencies. At the nominal value of the stiffness, the resonant frequency of the drive mode coincided with the structural fundamental frequency. The plots show that the nominal stiffness is

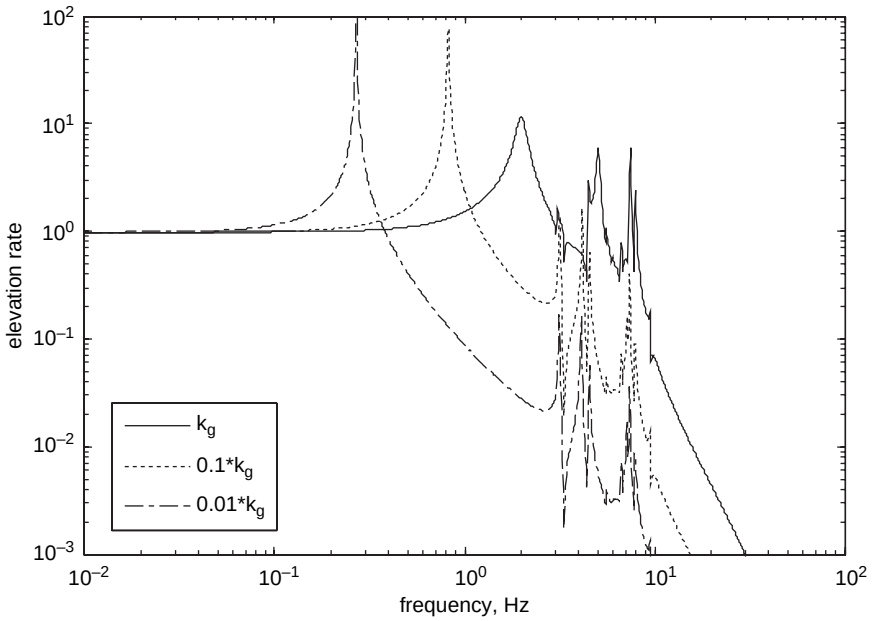

Fig. 2.12 The magnitudes of the transfer function of the velocity loop model for the nominal and decreased gearbox stiffness

slightly too low, because the inreased gearbox stiffness increased the velocity loop bandwidth.

Next, the gearbox stiffness is decreased by factors of 0.1 and 0.01, and the corresponding transfer functions are shown in Fig. 2.12 as dotted and dot-dashed lines, respectively. One can see that the transfer function bandwidth changed significantly. The resonant peak, related to the drive vibration mode is shifted to lower frequencies, impacting the bandwidth. The plots show that the nominal stiffness should not be decreased, because the lower gearbox stiffness impacts the velocity loop bandwidth.

2.5.2 Drive Inertia Factor

Here, the impact of the motor inertia on the velocity loop properties is investigated. The transfer function from the velocity command to the output velocity for the nominal inertia is shown in Fig. 2.13, solid line. First, the motor inertia is decreased by factors 0.1 and 0.01, and the corresponding transfer functions are shown in Fig. 2.13, dotted and dot-dashed lines, respectively. One can see that the transfer function bandwidth changed insignificantly. The resonant peak, related to the drive vibration mode shifted to higher frequencies. The plots show that the nominal inertia

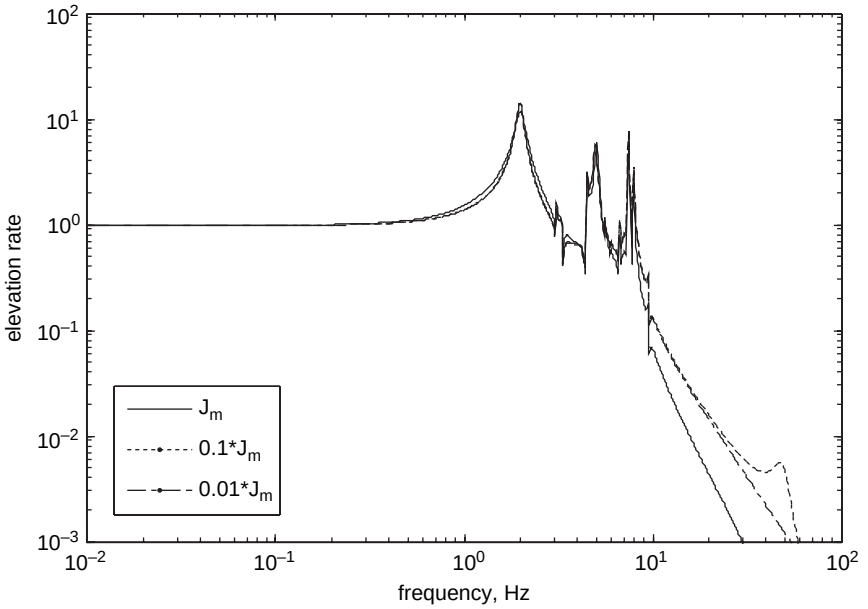

Fig. 2.13 The magnitudes of the transfer function of the velocity loop model for the nominal and decreased motor inertia

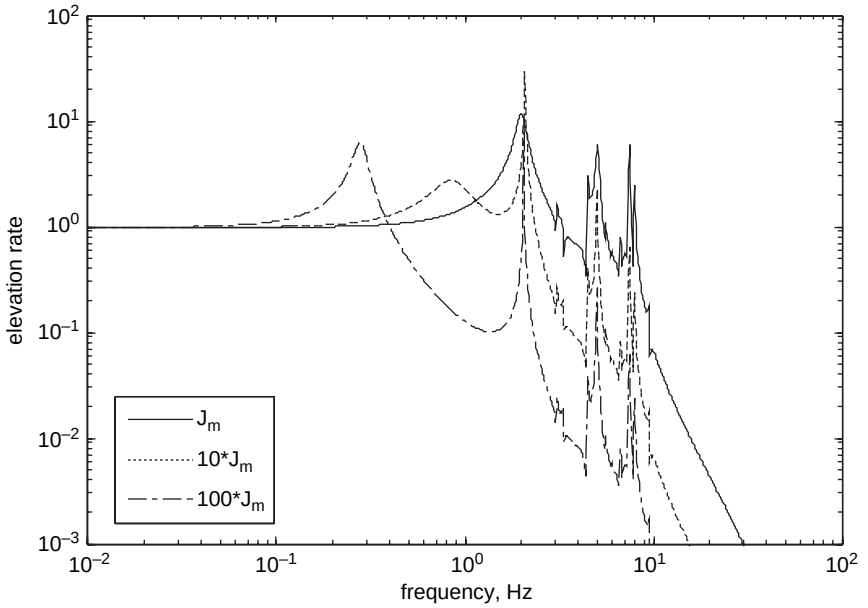

Fig. 2.14 The magnitudes of the transfer function of the velocity loop model for the nominal and increased motor inertia

is sufficient, because the lower motor inertias does not impact the velocity loop bandwidth.

Next, the motor inertia is increased by factors 10 and 100, and the corresponding transfer functions are shown in Fig. 2.14, dotted and dot-dashed lines, respectively. In this case the transfer function bandwidth changed significantly. The resonant peak related to the drive vibration mode is shifted to the lower frequencies, impacting the bandwidth. Note that the antenna fundamental frequency has not been changed. The plots show that the nominal inertia cannot be increased, because it impacts the velocity loop bandwidth.

This simple investigation shows that the gearbox stiffness has its lower limit that should not be violated, because it impacts the velocity loop bandwidth and the closed loop performance. Similarly, the motor inertia has its upper limit. The limit is defined by the antenna fundamental frequency: drive natural frequency should be at least the fundamental frequency of the structure.

References

1. Franklin GF, Powell JD, Workman ML. (1992). *Digital Control of Dynamic Systems.* Addison-Wesley, Reading, MA.
2. Gawronski W. (2004). *Advanced Structural Dynamics and Active Control of Structures*. Springer, New York.
3. Gawronski W, Mellstrom JA. (1992). A Parameter and Configuration Study of the DSS-13 Antenna Drives. *TDA Progress Report*, No.42-110, available at http://ipnpr.jpl.nasa.gov/progress_report/42-110/110S.PDF.
4. Lim KB, Gawronski W. (1996). Hankel Singular Values of Flexible Structures in Discrete Time," *AIAA J. Guidance, Control, and Dynamics*, 19(6):1370–1377.